Available online at www.sciencedirect.com
SCIENCE DIRECT®
Ocean Engineering 31 (2004) 177–199
OCEAN ENGINEERING
www.elsevier.com/locate/oceaneng

Optimum design of multiple intersecting spheres deep-submerged pressure hull

Cho-Chung Liang [a,*], Sheau-Wen Shiah [b], Chan-Yung Jen [c], Hung-Wen Chen [d]

[a] *Department of Mechanical and Automation Engineering, Da-Yeh University, 112. Shan-Jiau Road, Da-Tsuen, Chang-Hua 515, Taiwan, ROC*
[b] *Department of Naval Architecture and Marine Engineering, University of National Defense Chung Cheng Institute of Technology, Ta-Shi, Tao-Yuan 335, Taiwan, ROC*
[c] *Institute of System Engineering, University of National Defense Chung Cheng Institute of Technology, Ta-Shi, Tao-Yuan 335, Taiwan, ROC*
[d] *Chung-Shan Institute of Science and Technology, Lung-Tan, Tao-Yuan 335, Taiwan, ROC*

Received 23 January 2003; accepted 14 May 2003

Abstract

The multiple intersecting spheres (MIS) pressure hull is a logical derivative of the single unstiffened sphere, which is frequently used for deep operating, small submersibles because of its attractive low buoyancy factor. This paper investigates the optimum design of an MIS deep-submerged pressure hull subjected to hydrostatic pressure, using a powerful optimization procedure combined the extended interior penalty function method (EIPF) with the Davidon–Fletcher–Powell (DFP) method. In this study, the thickness of the shell, the width of the rib-ring, the inner radius of the rib-ring and the angle of intersection of the spherical shell are selected as design variables, and structural failure and human requirements are considered to minimize the buoyancy factor. Additionally, a sensitivity analysis is performed to study the influence of the design variables on the optimal structural strength design. The results reveal that the shell thickness is most important to lobar buckling strength, and that rib-ring width, rib-ring inner radius and spherical shell intersection angle are most important to rib-ring hoop strength. Optimization results may provide a valuable reference for designers.

Keywords: Optimization; Multiple intersecting spheres; Pressure hull; DFP; EIPF

* Corresponding author. Tel.: +886-4-8511220; fax: +886-4-8511224.
E-mail address: ccliang@mail.dyu.edu.tw (C.-C. Liang).

0029-8018/$ - see front matter
doi:10.1016/S0029-8018(03)00120-3

1. Introduction

Deep-diving submersible vehicles (DSVs) are widely used for diverse military and commercial applications, ranging from rescuing submarines, hunting mines and gathering intelligence, to laying underwater cables, exploring oceanographic resource and monitoring pollution. In service, DSVs are designed to operate at depths of 600–6000 m, at which they can cover over 98% of the ocean's floor. Therefore, a submersible pressure hull must endure extreme hydrostatic pressure and, simultaneously carry a maximum payload of a crew and necessary equipment. The pressure hull is the main structure of a DSV, and frequently constitutes one-quarter to one-half and more of the total weight of the vehicle (Reynolds et al., 1973). One of the major problems confronted by the designer of deep submersibles is to minimize the weight of the pressure hull, that is, to increase the payload, propulsion, and life support for the hull with the lowest weight to buoyancy ratio at a given depth. These improvements can be achieved through the advanced hull concept and/or efficient material systems. However, this work focuses on designing a novel geometrical configuration by considering the buoyancy factor. Hull design includes a long and successful history of cylindrical and spherical pressure hulls for DSVs. The sphere is the most efficient and simple shape for a hull to resist external hydrostatic pressure. Structurally, it has the lowest weight per unit volume, but a spherical shape offers less internal space for housing personnel and equipment than a long circular cylinder with the same internal diameter. Hydrodynamically, however, a cylindrical hull that has a suitable length-to-diameter ratio has a better internal arrangement and lower fabrication cost. During recent years, a dramatic design of deep submersibles involved multiple intersecting spheres (MIS), as shown in Fig. 1. It includes a series of spheres that are reinforced at their intersections by reinforcing rings. Such an attractive hull construction has the advantages of the both the cylindrical hull and the spherical hull; it will be a simpler, safer and more economical pressure hull for DSVs in the future (Allmendinger, 1990). Given the wide range of applications of DSVs and the innovation of the multiple intersecting spheres design, this paper addresses the design problem of optimizing a multiple intersecting spheres deep-submerged pressure hull, considering various structural strength constraints under hydrostatic pressure. Additionally, the buoyancy factor, B, defined as the weight-to-displacement ratio of the pressure hulls, reflects the geometrical efficiency characteristics of the pressure hull for DSVs and is also studied in detail. This factor is employed to evaluate the structural efficiencies of the various pressure hulls. This study proposes the buoyancy factor as an alternative to the performance factor as the objective function in the design problem of optimizing the multiple intersecting spheres pressure hull.

Several major studies have been undertaken on the design of the DSV pressure hull. Modern submersible development began in the early 1930s, motivated principally by scientific research interests. The bathysphere Trieste made her historic dive to 10,915 m in the Mariana Trench, for 20 min, on January 23, 1960, finding marine life at this depth. No submersible has again reached this record depth (Muukki, 1990). Mckee (1959) thoroughly described the displacement, weight, external shape

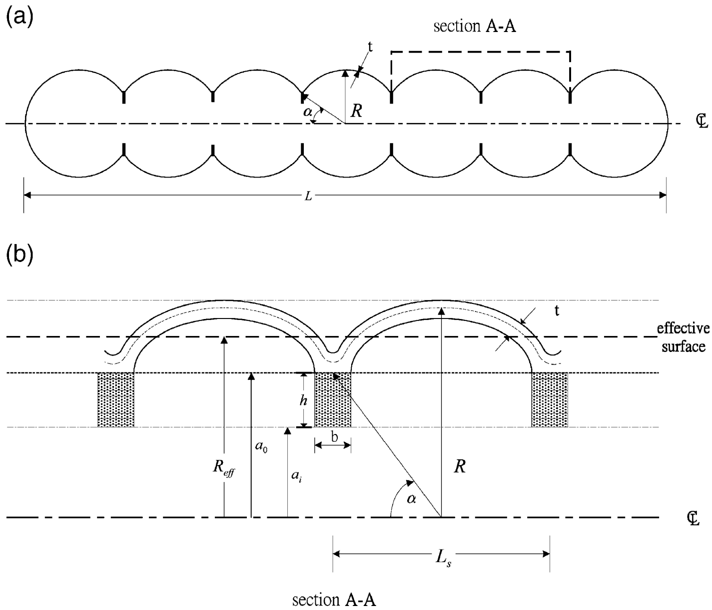

Fig. 1. Geometry of a multiple intersecting spheres (MIS) deep-submerged pressure hull. (a) Gas-storage toroidal tube-stiffener hull wall construction. (b) Trapezoid corrugated hull wall construction. (c) Ring-stiffened corrugated hull wall construction.

and structure of US and German submarines used in World War II. According to Mckee's investigation, the spherical pressure hull offers a better strength/weight ratio than a cylinder and cone. Garland (1968) presented the design requirements and fabrication procedures used to construct the pressure hull of a deep submergence vehicle. He asserted not only does the weight/buoyancy ratio plays an important role in determining the payload of a DSV pressure hull, but also that a higher strength material requires less weight and provides more buoyancy, increasing a higher permitted payload. Moreover, in Garland's study, the selection of high specific strength materials preceded all other considerations in developing pressure hulls of deep-diving vehicles. Shankman (1968) thoroughly described striking differences among several various alloys and processes and appraised the feasibility of related applications. His investigation also indicated that increasing the design depth depends on a corresponding increase in the thickness of the hull and the weight/displacement ratio. Watson (1971) presented the design, construction and operational experiences of the "GUPPY" deep-diving submersible vehicle, constructed as a single sphere. According to his results, the structural failure attributed to the buckling of a shell may occur at nominal stresses far below the yield strength of the material. Leon (1971) presented and tested an intersecting sphere (bi-spherical) configuration of titanium alloy that had been used as a deep submergence pressure hull model. The results revealed that a weight saving of 10% of the payload could be obtained by replacing the titanium-reinforced ring by the high strength, lightweight ceramic (Al_2O_3) in the bi-spherical configuration. Harris (1977) suggested that a circumferential tube-stiffened construction shown in Fig. 2a is another alterative to the traditional ring-stiffened cylindrical pressure hulls; however, circumferential shell buckling often occurs to such construction. Heggstad (1982) presented that the weight-to-displacement ratio of pressure hulls optimized according to steel quality and maximum operating depth. He also showed that the maximum speed was obtained by improving the quality of the steel in relation to the maximum operating depth. Ross (1987) presented an alternative design to the traditional ring-stiffened cylindrical pressure hull; it was the corrugated hull wall, shown in Fig. 2b. Ross pointed out that the corrugated pressure hull is structurally

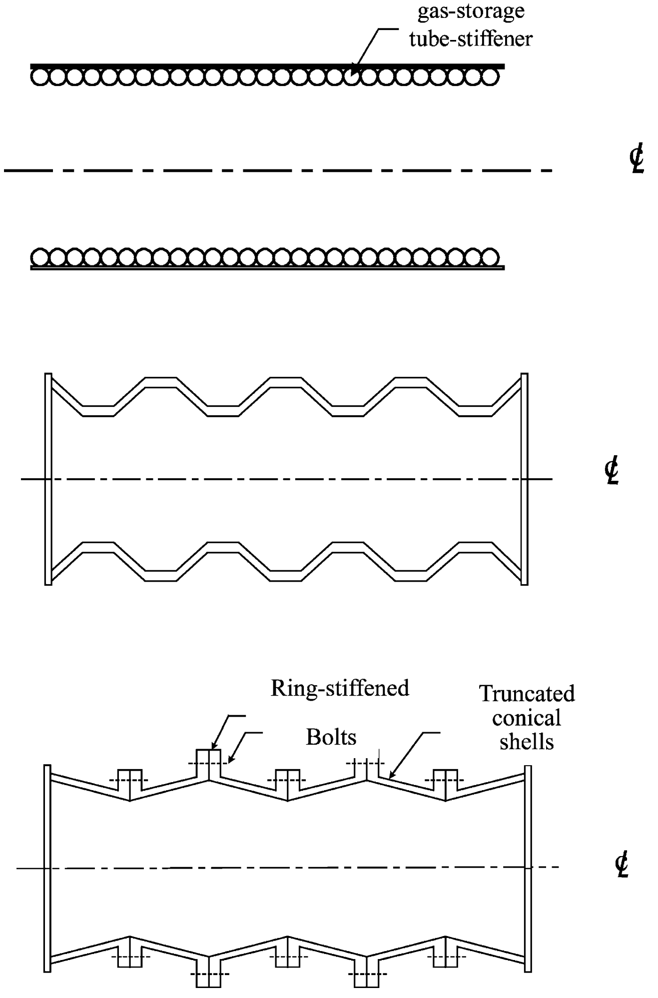

Fig. 2. Ross's three different configuration hull wall construction.

more efficient than the traditional ring-stiffened equivalent of the same volume and weight. Yuan et al. (1991) presented a theoretical analysis of the elastic general instability of two swedged-stiffened cylinders subjected to hydrostatic pressure loading. They studied the effect of varying the angle of the cone section on this general instability pressure. Yuan's study proposes a reasonable cone angle range for swedged-stiffened cylinders, considering structural buckling, available cabin space and weight reduction. Additionally, Hall et al. (1991) proposed that the graphite/epoxy composite intersecting spheres design achieved a weight saving of 46% of that of steel intersecting spheres with the same diameter. Yang et al. (1992) conducted a search for the optimal form of torispherical dome ends under an external pressure load. In Yang's work, a minimum weight optimization problem was studied by using the discrete backtrack programming method; the optimal forms were obtained considering buckling constraints. The developed optimal search procedure was improved to be very efficient and easy-to-use for applications in his study. In addition to reviewing manned and unmanned submersible vehicle systems, Garzke et al. (1993) highlighted the importance of the systems in the exploration of the geology of the ocean bottom and underwater wrecks, such as the Titanic and Bismarck. Garzke et al. asserted that the development of deep-diving manned/unmanned submersibles could lead to a new architectural field. Ross (1996) described how it is possible to manufacture a full-scale corrugated submarine pressure hull, by building it in segments, as shown in Fig. 2c. Liang et al. (1997) proposed a minimum weight design of a submarine pressure hull under hydrostatic pressure subjected to some constraints, such as general instability, buckling of shell between frames, plate yielding, and frame yielding. Ness and Simpson (2000) offered the unique combination of submarine external shape with elliptical cross-sections and the pressure hull of clustered intersecting spheres to reduce the surface area of the traditionally shaped submarine without increasing hull depth. Liang and Chen (2002) investigated the structural optimization of fiber-reinforced sandwich cylindrical pressure hulls subjected to external hydrostatic pressure loading. In Liang's work, the optimal composite shell configuration was obtained using an advanced discrete optimization technique.

Although the above investigations have provided numerous preliminary results related to the minimum weight design of deep-diving submersible vehicles with cylindrical, conical and dome shells, very few theories, collateral test results and techniques for applying the design to multiple intersecting spheres have been reported. This gap in information is due to the relatively small number of engineers and scientists engaged in this limited field. Furthermore, Leon's (1971) work and Hall's (1991) work are concerned only with the effects of the different hull materials to reduce the weight of the pressure hulls. Their work does not discuss the optimal configuration design of multiple intersecting sphere pressure hull.

Accordingly, this study aims to maximize the structural efficiency of a multiple intersecting spheres deep-submerged pressure hull under hydrostatic pressure. Some mechanical behavior constraints are considered in this paper. These constraints include the compatibility of deformation between the shell and the stiffened rib-ring, lobar buckling and the strength of the shell, crippling and the strength of the rib-ring, and the overall buckling of the pressure hull. Additionally, human and spatial requirements are considered. The buoyancy factor is employed to evaluate the structural efficiency of a deep-submerged pressure hull. Design variables used in the present optimal formulation include shell thickness, rib-ring width, rib-ring inner radius and the intersection angle of the spherical shells. Therefore, the presently considered optimal design problem involves determining the best geometrical configuration for minimizing the buoyancy factor of the pressure hull. An optimization procedure is implemented to solve this constrained optimization problem: the extended interior penalty technique is utilized to transform the constrained original objective function into the unconstrained modified objective function. Then, the Davidon–Fletcher–Powell (DFP) method is employed to minimize the unconstrained modified objective function. Finally, an optimum design is presented and investigated. A sensitivity analysis is performed to study the effects of the design variables on the optimal design. The optimal configuration of a multiple intersecting spheres deep-submerged pressure hull that minimizes the buoyancy factor is presented. The degree of influence of the design variables on the structural strength was also estimated. Some favorable results are presented to provide a valuable reference for designers of deep-diving submersible vehicles.

2. Multiple intersecting spheres and design considerations

Various pressure vessel configurations were designed and built for submersibles. The most prevalent ones are stiffened cylinders with hemispherical heads and single spheres. Recently, a novel shape, built from MIS, has been built (see Fig. 1). It is a logical derivative of the unstiffened single sphere design. MIS stiffened at their intersections have very attractive features. The buoyancy factor is low; the shape is more attractive than a single sphere for hydrodynamic fairing, and the suitable length-to-diameter ratio is more favorable for the internal and external arrangements.

2.1. MIS configuration

MIS involves a series of spheres, reinforced at their intersections by reinforcing rings. These reinforcing rings can be made either of the same material as the spherical shell, or of a material that is stronger and has a greater elastic modulus. The latter alternative results in a considerably better buoyancy factor B, since the substantial weight of the reinforcing ring is reduced. The annular area of the reinforcing ring is also smaller, allowing for a larger access path between spheres. Costs may be attractive too, since the rings are a small part of the total weight of the hull. The principal structural members of the MIS pressure configuration are several stiffened spherical sections and two end-closure spherical bulkheads. The shell thickness t, the shell middle surface radius R, the shell intersection angle α, and the entire length L are defined as in Fig. 1a. The major structural components of the MIS pressure hull are the shell plating and the shell stiffeners (rib-rings). The rib-ring width b, the rib-ring inner radius a_i, the rib-ring outer radius a_o, the rib-ring height h, the rib-ring spacing L_s, and the average effective radius R_{eff} are also defined as in Fig. 1b.

2.2. Strength analysis of MIS pressure hull (Allmendinger, 1990)

A deep-diving submersible may descend to near the bottom of the sea for exploration or rescue. Therefore, the pressure hull must bear a very high hydrostatic pressure and endure extreme stress, which may exceed the material yielding strength; crippling, lobar and global buckling may occur. The geometrical and mechanical behavior effects must be considered as follows to avoid the aforementioned major failure modes and provide the preferable structural efficiency.

2.2.1. Buoyancy factor B of the MIS

The common basis for evaluating the structural efficiencies of the various hulls is the buoyancy factor, defined as the hull weight to displaced water weight ratio. The buoyancy factor of the MIS is

$$B = \frac{3\left[nW_r + 4\pi R^2 t\rho_s(n\cos\alpha + 1)\right]}{4\pi R^3\rho_w[(n\cos\alpha)(1 + 1/2\sin^2\alpha) + 1]}, \tag{1}$$

where

$$W_r = [b(a_o - a_i)]\left[R\sin\alpha - \frac{1}{2}(a_o - a_i)\right]2\pi\rho_r = \pi b R^2\sin^2\alpha\left(1 - C^2\right)\rho_r,$$

W_r is the weight of rib-ring, a_i the inner radius of rib-ring, a_o the outer radius of rib-ring, $a_o = R\sin\alpha$, n the number of rib-rings, C the ratio of inner radius/outer radius of the rib-ring, $C = a_i/a_o$, ρ_s the density of the shell, ρ_r the density of the rib-ring, and ρ_w the density of sea water ($\rho_w = 1025$ kg/m^3 is used herein).

2.2.2. Displacement of shell's membrane in MIS

The component of the displacement of the shell's membrane normal to the axis of revolution is

$$\delta_s = \frac{PR^2\sin\alpha}{2tE_s}(1 - \mu_s), \tag{2}$$

where P is the hydrostatic pressure, E_s the elastic modulus of the spherical shell, and μ_s Poisson's ratio of the spherical shell.

2.2.3. Deflection of the rib-ring at the intersection of the MIS shell

The deflection of the rib-ring at the intersection of the shell is

$$\delta_r = \frac{PR^2\sin\alpha\cos\alpha}{E_r b}\left(\frac{1 + C^2}{1 - C^2} - \mu_r\right), \tag{3}$$

where E_r is the elastic modulus of the rib-ring, and μ_r Poisson's ratio of the rib-ring.

2.2.4. Membrane stress of MIS shell

According to Allmendinger (1990), the membrane stress (σ_{memb}) in the shell is

$$\sigma_{\mathrm{memb}} = \frac{PR}{2t} \tag{4}$$

2.2.5. Stress in the rib-ring at its inner radius

The stress in the rib-ring (σ_{r}) at its inner radius is

$$\sigma_{\mathrm{r}} = \frac{2PR\cos\alpha}{b(1-C^2)} \tag{5}$$

2.2.6. Lobar buckling in the MIS shell

Lobar buckling in the spherical shell of an MIS pressure hull is herein considered to prevent local failure. Lobar buckling is based on a systematic series of tests of hydrostatically loaded shallow spherical caps, as presented by Kloppel and Jungbluth (Nash, 1995). The empirical expression for hydrostatic buckling pressure is

$$P_{\mathrm{crL}} = \left[1 - 0.175\left(\frac{70^{\circ} - \alpha}{20^{\circ}}\right)\right]\left[1 - 0.07\left(\frac{R}{400\ t}\right)\right]\left(0.3\ E_{\mathrm{s}}\frac{t^2}{R^2}\right), \tag{6}$$

where α and R are defined in Fig. 1; t represents the thickness of the shell, and P_{crL} is the pressure for initiating formation of the first lobe.

2.2.7. Crippling in the rib-ring

The crippling constraint on the rib-ring ensures the stability of the rib-ring component herein. The optimum (weightwise) proportions of hull stiffeners will be those for which the outstanding flanges (or web) will cripple at the material yield point. According to Gorman and Louie (1991), the rib-ring crippling analysis can be cast in the form

$$F_{\mathrm{crit}} = K_{\mathrm{c}}E_{\mathrm{r}}\left(\frac{b}{h}\right)^2, \tag{7}$$

where F_{crit} is crippling buckling stress of the rib-ring, K_{c} a geometry and condition-dependent coefficient ($K_{\mathrm{c}} = 6.35$ is adopted in this paper).

2.2.8. General instability

The MIS pressure hull is similar to the stiffened cylindrical one. Therefore, an effective general instability of the MIS pressure hull is considered herein, based on the general instability of the stiffened cylindrical shell that was developed by Kendrick and modified by Bryant (Comstock, 1967). Such an effective general instability is obtained by modifying the general instability of a stiffened cylindrical shell. Accordingly, the expression for the critical general buckling pressure of pressure hull with multiple intersecting spheres is (Fig. 1b)

$$P_{\mathrm{cr}} = \frac{E_{\mathrm{s}}t}{R_{\mathrm{eff}}}\left[\frac{m^4}{\left(n_{\mathrm{m}}^2 + (m^2/2) - 1\right)\left(n_{\mathrm{m}}^2 + m^2\right)^2}\right] + \frac{\left(n_{\mathrm{m}}^2 - 1\right)E_{\mathrm{s}}I}{R_{\mathrm{eff}}^3 L_{\mathrm{s}}}, \tag{8}$$

where,

$$R_{\mathrm{eff}} = R/2(1 + \sin\alpha),$$

$$L_{\mathrm{s}} = 2R\cos\alpha,$$

$$m = \pi R_{\mathrm{eff}}/L_{\mathrm{s}},$$

$$I = (hb(h/2 + t/2)^2/1 + (h/L_{\mathrm{s}})(b/t)) + \frac{bh^3}{12} + \frac{L_{\mathrm{s}}t^3}{12},$$

I is the moment of inertia of the frame, n_{m} is the buckling mode shape ($n_{\mathrm{m}} = 1 - 10$).

3. Optimization formulation of MIS pressure hull

An externally pressurized MIS pressure hull is designed to yield the minimum buoyancy factor to satisfy design requirements. The optimization design is mathematically modeled as follows.

3.1. Design variables

The pre-assigned design parameters are the number (n) of rib-rings, the middle surface radius of the shell (R), and the material properties of both. The thickness (t) of the shell, the width (b) of the rib-ring, the inner radius (a_{i}) of the rib-ring and the angle (α) of the shell intersection are taken as the design variables for the optimization problem. Then, the design variables of the MIS pressure hull can be stated as: the design variable vector $X = (x_1,\ x_2, \ldots, x_N)$, $N = 4$, design variables $x_1 = t$, $x_2 = b$, $x_3 = a_i$, $x_4 = \alpha$ (Fig. 1).

3.2. Objective function

The optimal design problem involves determining the best geometrical configuration for minimizing the buoyancy factor of the MIS pressure hull under hydrostatic pressure. The objective in the design of an MIS deep-submerged pressure hull is to minimize the buoyancy factor, equivalent to maximizing structural efficiency. The buoyancy factor, B, is regarded as the objective function $F(X)$ and is stated as follows.

$$\min.\ F(X) = B = \frac{3\left[nW_{\mathrm{r}} + 4\pi R^2 t\rho_{\mathrm{s}}(n\cos\alpha + 1)\right]}{4\pi R^3\rho_{\mathrm{w}}[(n\cos\alpha)(1 + 1/2\sin^2\alpha) + 1]} \tag{9}$$

3.3. Design constraints

The constraining equations can be classified into three groups—behavior constraints that control the failure modes, geometrical constraints to specify spatial and human requirements and side constraints that specify the permissible range of design variables. Such constraints are presented as follows.

3.3.1. Behavior constraints

In order to ensure the structural stability, the failure and strength constraints imposed on the deep-submerged pressure hull must be satisfied. In this paper, several failure and strength criteria are used as behavior constraints. These constraints are described below.

3.3.1.1 Compatibility of deformation. The criterion utilized in the preliminary sizing of the intersecting rib-ring involves matching the shell displacements with the rib-ring displacements to avoid the induction of large bending stresses in the shell. The shell deflection is accordingly set equal to the rib-ring deflection at their intersection (Allmendinger, 1990). Therefore,

$$\frac{\cos\alpha}{E_{\mathrm{r}}b}\left(\frac{1+C^2}{1-C^2}-\mu_{\mathrm{r}}\right)=\frac{(1-\mu_{\mathrm{s}})}{2tE_{\mathrm{s}}} \tag{10}$$

Accordingly, the compatibility of deformation is ensured by satisfying the following equality constraint.

$$l_1:\frac{E_{\mathrm{r}}b}{2tE_{\mathrm{s}}\cos\alpha}\,\frac{(1-\mu_{\mathrm{s}})(1-C^2)}{[(1+C^2)-\mu_{\mathrm{r}}(1-C^2)]}-1=0 \tag{11}$$

3.3.1.2 Material strength constraint. In order to avoid materials yielding in the shell and rib-ring, the stress of the shell and rib-ring is considered to be less than its material yielding strength, respectively. Hence, the strength inequality constraint on the shell and in the rib-ring can be expressed as,

$$g_1:\frac{\sigma_{\mathrm{memb}}}{\sigma_{\mathrm{s}}^{\mathrm{y}}}-1\leq 0,\quad \text{or}\quad g_1:K_{\mathrm{m}}^{\mathrm{s}}-1\leq 0, \tag{12}$$

$$g_2:\frac{\sigma_{\mathrm{r}}}{\sigma_{\mathrm{r}}^{\mathrm{y}}}-1\leq 0,\quad \text{or}\quad g_2:K_{\mathrm{m}}^{\mathrm{r}}-1\leq 0, \tag{13}$$

where $\sigma_{\mathrm{s}}^{\mathrm{y}}$ is the yielding strength of shell, $\sigma_{\mathrm{r}}^{\mathrm{y}}$ the yielding strength of rib-ring, $K_{\mathrm{m}}^{\mathrm{s}}$ the shell strength factor, which is the ratio of the membrane stress in the shell to its material yielding strength, $K_{\mathrm{m}}^{\mathrm{s}}=\sigma_{\mathrm{memb}}/\sigma_{\mathrm{s}}^{\mathrm{y}}$, and $K_{\mathrm{m}}^{\mathrm{r}}$ the rib-ring strength factor, which is the ratio of the rib-ring stress at the inner radius to its material yielding strength, $K_{\mathrm{m}}^{\mathrm{r}}=\sigma_{\mathrm{r}}/\sigma_{\mathrm{r}}^{\mathrm{y}}$.

3.3.1.3 Shell lobar buckling constraint. The lobar buckling pressure P_{crL} in the spherical shell of MIS pressure hull must be higher than operating load P and its constraint is,

$$g_3:\frac{P}{P_{\mathrm{crL}}}-1\leq 0,\quad \text{or}\quad g_3:K_{\mathrm{L}}-1\leq 0, \tag{14}$$

where K_{L} is the shell lobar buckling strength factor, which is the ratio of the hydrostatic pressure to the lobar buckling strength of the shell, $K_{\mathrm{L}}=P/P_{\mathrm{crL}}$.

3.3.1.4 Rib-ring crippling constraint. The maximum applied external pressure must be less than the rib-ring compressive buckling stress F_{crit} to prevent the crippling buckling of the rib-ring. The constraint is,

$$g_4 : \frac{P}{F_{\text{crit}}} - 1 \leq 0, \quad \text{or} \quad g_4 : K_{\text{crip}} - 1 \leq 0, \tag{15}$$

where K_{crip} is the rib-ring crippling strength factor, which is the ratio of the hydrostatic pressure to the crippling strength of the rib-ring, $K_{\text{crip}} = P/F_{\text{crit}}$.

3.3.1.5 General instability constraint. Notably, P_{cr} must be the minimum global buckling of the MIS pressure hull from buckling mode shapes ($n_{\text{m}} = 1 - 10$). Also, P_{cr} must exceed the operating loading to ensure the stability of the pressure hull. Therefore, a general instability of MIS pressure hull is presented as,

$$g_5 : \frac{P}{P_{\text{cr}}} - 1 \leq 0, \quad \text{or} \quad g_5 : K_{\text{O}} - 1 \leq 0, \tag{16}$$

where K_{O} is the overall buckling strength factor, which is the ratio of the hydrostatic pressure to the overall buckling strength of the pressure hull, $K_{\text{O}} = P/P_{\text{cr}}$.

3.3.2. Geometrical constraints

In this paper, some geometrical constraints are considered to meet spatial and human requirements. These requirements include sufficient access between compartments for personnel and equipment and limiting rib-ring width. The geometrical constraints on the MIS pressure hull under external hydrostatic pressure load are described below.

Consider the height limitation of the rib-ring:

$$0 \leq h \leq \frac{1}{6} a_0,$$

where h is the rib-ring height, $h = a_{\text{o}} - a_{\text{i}}$.

Two geometries are specified as,

$$g_6 : \frac{5}{6} - C \leq 0, \tag{17}$$

and

$$g_7 : C - 1 \leq 0. \tag{18}$$

The limiting width of the rib-ring is,

$$0 \leq b \leq L_{\text{s}}.$$

Therefore, geometry is specified as,

$$g_8 : \frac{b}{2R\cos\alpha} - 1 \leq 0. \tag{19}$$

3.3.3. Side constraints

In addition, corresponding to the choice of the design variables, the following conditions of the dimensioning belong to the group of side constraints in this investigations:The thickness of the shell is,

$$t_{\min} \leq t \leq t_{\max} \tag{20}$$

The width of the rib-ring is,

$$b_{\min} \leq b \leq b_{\max} \tag{21}$$

The inner radius of the rib-ring is,

$$(a_{\mathrm{i}})_{\min} \leq a_{\mathrm{i}} \leq (a_{\mathrm{i}})_{\max} \tag{22}$$

The angle of intersection of the shell is,

$$\alpha_{\min} \leq \alpha \leq \alpha_{\max} \tag{23}$$

4. The solution algorithm

In this paper, the optimal design problem of MIS deep-submerged pressure hull is a nonlinear constrained optimization problem. Owing to the equality constraint considered in this optimization design problem, it is difficult to solve the design problem by direct method, such as the methods of feasible directions. Therefore, the extended interior penalty technique is used to transform the constrained original objective function into the unconstrained modified objective function. Accordingly, a powerful optimization procedure combined the extended interior penalty function method (EIPF) with the Davidon–Fletcher–Powell method (Vanderplaats, 1985) to solve the present nonlinear constrained optimization design problem of the MIS deep-submerged pressure hull herein.

In this study, the modified objective function based on such a technique is expressed as,

$$\phi(X, r_k) = F(X) - r_k \sum_{i=1}^{p} \frac{1}{g_i(X)} + \frac{1}{\sqrt{r_k}} \sum_{j=1}^{q} \left[l_j(X) \right]^2, \tag{24}$$

where $\phi(X, r_k)$ is the modified objective function, $F(X)$ the objective function, X the N-dimensional vector of design variables, $g_i(X)$ the a set of "p" inequality constraints, $i = 1$ to p, $l_j(X)$ a set of "q" equality constraints, $j = 1$ to q, r_k a positive constant penalty parameter, $r_{k+1} = \gamma r_k$, $\gamma = 0.1$, $(k = 1, 2, \ldots)$, p the number of inequality constraints, and q the number of equality constraints.

An appealing feature of this technique is that it produces an improving sequence of acceptable designs. Accordingly, this technique ensures the feasible design in each iterative procedure and allows comparing sub-optimal designs to the optimum one in this paper. The DFP method is employed as an optimizer to search for the optimal designs. The DFP search routine based on the quasi-Newton method is one of the most efficient unconstrained minimization techniques. It is much better than the steepest descent method and somewhat more efficient than the conjugate gradient method. The method provides a good approximate inverse of the Hessian matrix of the objective function, using only the first derivatives. This modification is to overcome the pitfalls in the direct Newton's method.

Additionally, a symmetric rank-two update formula is used to update the old approximation matrix in the DFP search routine. The search method ensures a sequence of decreasing (improving) values of the objective function.

Fig. 3 shows the numerical optimization solution procedure. In such a procedure, first, the specific geometrical configuration of the MIS pressure hull, includ-

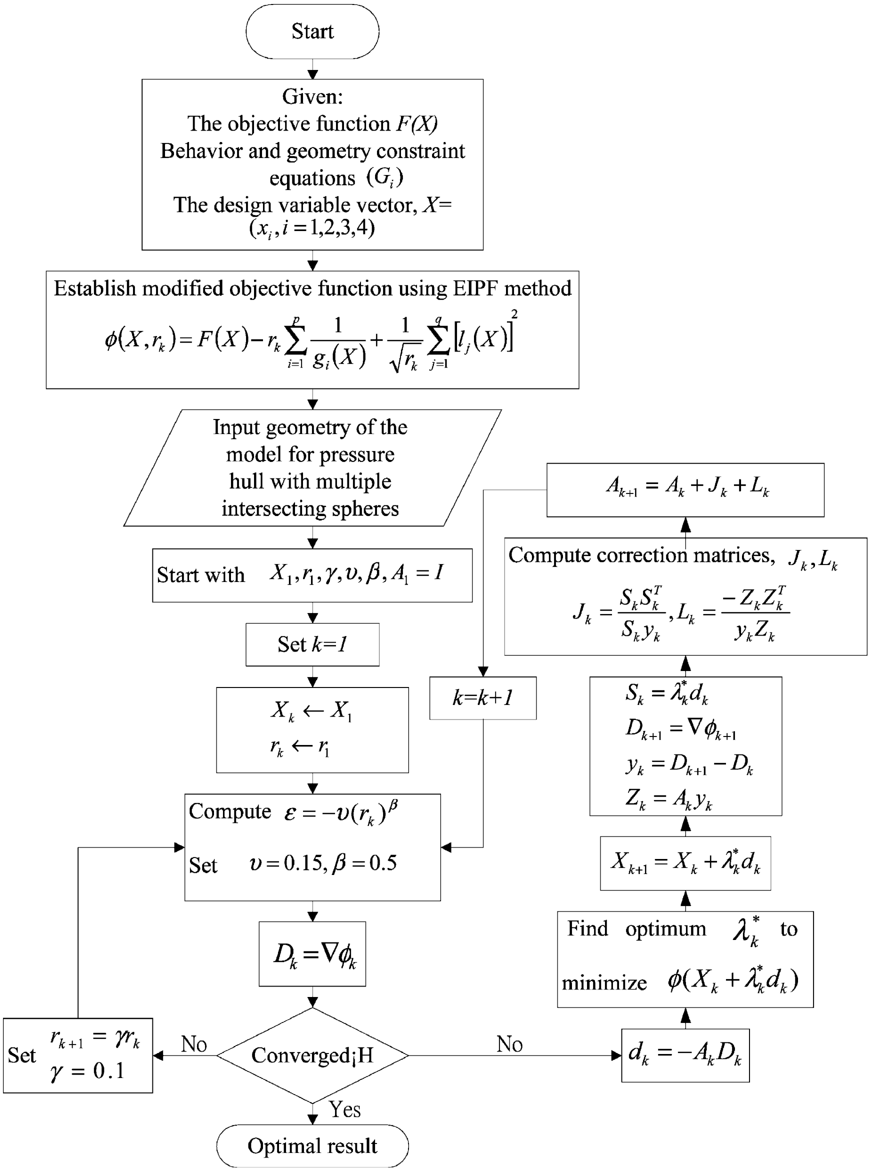

Fig. 3. An optimization solution procedure for MIS deep-submerged pressure hull.

ing the thickness (t) of the shell, the width (b) of the rib-ring, the inner radius (a_i) of the rib-ring and the angle (α) of the shell intersection, is assigned as a set of initial design variables in the optimization procedure. Additionally, the EIPF method is employed to convert the present constrained optimization problem into an unconstrained problem by combining the buoyancy factor function with behavior and geometrical constraints. Then, the DFP search routine chooses an initial symmetric positive definite matrix A_1 as an estimate for the inverse of the Hessian of the cost function and defines the initial search direction as d_k. Concurrently, the golden section method is adopted to determine an optimum step size λ_k^*, which can minimize $\phi(X, r_k)$ along the searching direction. The above iteration procedures are repeated until a termination criterion is satisfied.

5. Optimum design of MIS deep-submerged pressure hull

The MIS pressure hull of a DSV is considered as an example of an optimum design using DFP combined with EIPF. The structure shown in Fig. 1 is to be designed to achieve the minimum buoyancy factor needed to resist a high external hydrostatic pressure. Furthermore, the MIS pressure hull design must satisfy behavior constraints as described in Eqs. (11)–(23). According to the David Taylor Model Basin test results (Gertler, 1950), an optimal hydrodynamic maneuvering form, of which the length to diameter ratio is approximately 6:1, is adopted. Additionally, the MIS model recommends that the middle surface of the sphere shell should have a diameter of 2.0 m, based on the human factors engineering analysis (Takagawa, 1995). The MIS pressure hull is constructed using HY-100 high strength steel and reinforced at its intersections by six rib-rings of the same material.

6. Principal geometrical dimensions and material properties

The principal geometrical dimensions of the MIS pressure hull and the material properties of the HY-100 steel are described as follows:

1. Radius of the sphere shell middle surface: $R = 1.0$ m
2. Number of rib-rings: $n = 6$
3. Modulus of elasticity: $E = 210$ Gpa
4. Yielding strength: $\sigma_y = 690$ MPa
5. Ultimate strength: $\sigma_U = 793.5$ MPa
6. Density: $\rho = 7828$ kg/m^3
7. Poisson ratio: $\mu = 0.29$
8. Diving depth and hydrostatic pressure: 3000 m, i.e. $P = 30.165$ MPa.

The side constraints are,

$$0.001 \text{ m} \leq t \leq 0.10 \text{ m}$$

$$0.001 \text{ m} \le b \le 0.10 \text{ m}$$

$$0.001 \text{ m} \le a_i \le 0.90 \text{ m}$$

$$30^\circ \le \alpha \le 70^\circ.$$

6.1. Optimal design results and discussion

Results obtained using the above EIPF and DFP optimization procedure are presented. Tables 1 and 2 and Figs. 5–8 summarize the results of the optimization. Table 1 indicates that the optimal design point is $(t, b, a_i, \alpha) = (0.0220 \text{ m}, 0.0835 \text{ m}, 0.7518 \text{ m}, 70^\circ)$, and the optimal objective function (buoyancy factor, B) is 0.6185. These results can overcome all structural failures at a diving depth of under 3000 m in the optimum configuration of the MIS deep-submerged pressure hull. Notably, the total length, L of the present design is shortest because the angle of the shell intersection is maximum. Additionally, this table also indicates that material yielding and shell lobar buckling must be firstly considered to avoid structural failure.

Furthermore, a sensitivity analysis is presented to understand thoroughly the effects of the design variables upon the structural strength of the MIS deep-submerged pressure hull under hydrostatic pressure. These dimensionless variables including B, t/R, b/R, a_i/R, α, K_m^r, K_m^s, K_L, K_{crip}, and K_O, are introduced in such a manner so as to simplify the expression of the strength. The results are described as follows.

6.1.1. Effect of buoyancy factor on design variables

A key factor in determining the payload of MIS is the buoyancy factor. The buoyancy factor is a parameter expressing the efficiency of the structure in terms of its ability to provide for an excess of displacement over that required to support its own weight. 1.0 is seen to be the critical value of the buoyancy factor, where the empty pressure hull is in a condition of neutral buoyancy with zero efficiency with respect to its ability to support other weights. Below and above 1.0, the empty pressure hull floats or sinks, possessing positive or negative efficiency, respectively.

Eq. (1) shows that the buoyancy factor B is directly proportional to each design variable (t, b, α) and the diagram resembles a straight line. The buoyancy factor B is inversely proportional to the other design variable (a_i) and the diagram resembles a vertical parabola, which opens downward, as shown in Fig. 4.

A larger shell thickness, rib-ring width and angle of intersection of the spherical shell all imply a higher buoyancy factor. A larger inner radius of the rib-ring implies a lower buoyancy factor; the lowest buoyancy factor corresponds to the strongest ability to increase payload when the shell thickness, rib-ring width, rib-ring inner radius and spherical shell intersection angle are those of the optimal design values.

Table 1
The results of the optimal design of the MIS deep-submerged pressure hull

Buoyancy factor B	Design variables				Structural strength (Pa)			Stress resultant (Pa)	
	Shell thickness, t (m)	Rib-ring width, b (m)	Rib-ring inner radius, a_i (m)	Shell-intersecting angle, α (deg)	Lobar buckling strength	Rib-ring crippling strength	Overall buckling strength	Rib-ring Stress at inner radius	Shell membrane stress
0.6185	0.0220	0.0835	0.7518	70	3.02×10^7	3.02×10^{11}	3.87×10^8	6.87×10^8	6.86×10^8

Table 2
Degree of influence of design variables on the structural strength

Design variables	Strength factor				
	The rib-ring strength factor (K_m^r)	The shell strength factor (K_m^s)	The lobar buckling strength factor (K_L)	The rib-ring crippling strength factor (K_{crip})	The overall buckling strength factor (K_O)
Shell thickness (t)	×	○○	○○○	×	○
Shell-intersecting angle (α)	○○○	×	○○	○	○
Rib-ring width (b)	○○○	×	×	○	○○
Rib-ring inner radius (a_i)	○○○	×	×	○	○○

○○○, high influence; ○○, middle influence; ○, low influence; ×, unaffected influence.

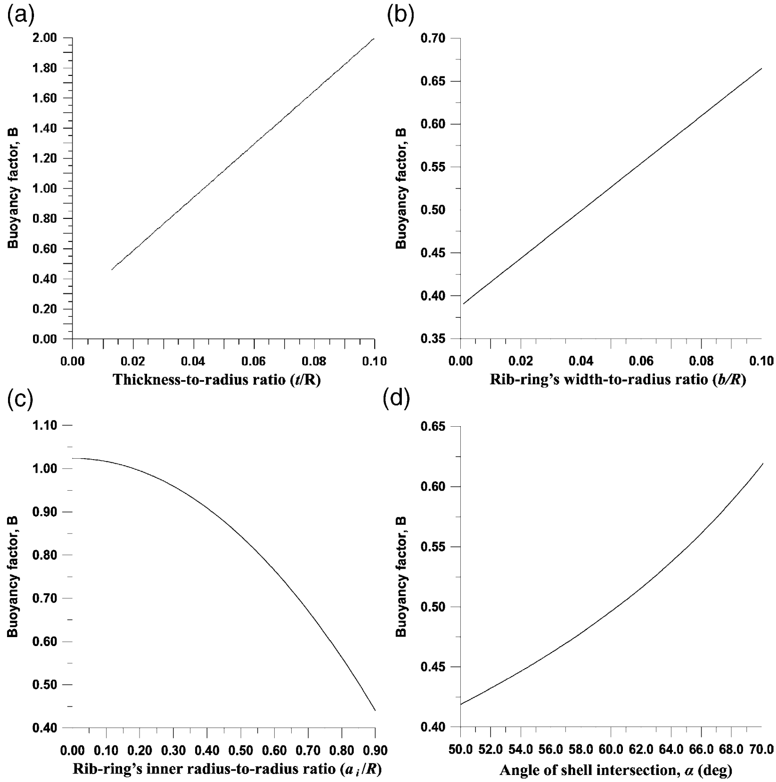

Fig. 4. The effect of buoyancy factor on design variables.

6.1.2. Effects of thickness-to-radius ratio (t/R)

Fig. 5 indicates the effects of thickness-to-radius (t/R) upon the structural strengths of the MIS deep-submerged pressure hull. The other three design variables are set at their optimal values. The following results are obtained.

The K_m^s curve shows that the shell membrane stress apparently decreases as t/R increases, and the maximum variation occurs in the range $t/R = 0.01$ to 0.05. If t/R is less than 0.022, the shell membrane stress will exceed its material yielding strength. Moreover, when the t/R exceeds 0.1, the shell membrane stress obviously stops decreasing. The K_L curve indicates that the lobar buckling strength in the shell heavily increases with t/R, and the maximum variation occurs in the range $t/R = 0.01$ to 0.05. If t/R is less than 0.022, then the lobar buckling strength cannot resist the external hydrostatic pressure load, inducing the local buckling of the shell. The K_O curve indicates that the overall buckling strength of the pressure hull does not apparently vary as t/R increases; that is, the effect of t/R on the overall buckling strength is not outstanding influence. Additionally, t/R does not affect the K_m^r and K_{crip} strength factors.

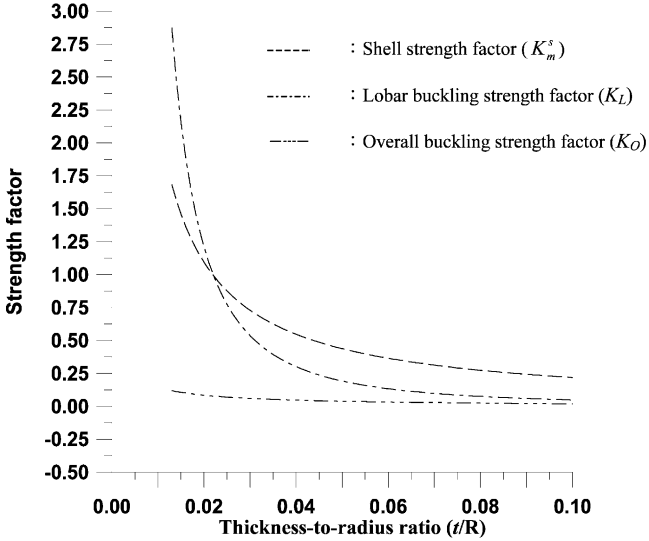

Fig. 5. The effects of thickness-to-radius (t/R) upon the structural strengths.

Accordingly, t/R strongly affects the shell membrane stress and the lobar buckling strength. However, the effects of t/R on the rib-ring stress, the rib-ring crippling strength and the structural overall buckling strength can be neglected. Therefore, the t/R can be appropriately chosen between 0.022 and 0.05 to obtain the minimum buoyancy factor; reduce the shell membrane stress and increase the lobar buckling strength.

6.1.3. Effects of rib-ring's width-to-radius ratio (b/R)

Fig. 6 indicates the effects of the rib-ring's width-to-radius ratio (b/R) upon the structural strengths of the MIS deep-submerged pressure hull, when the other three design variables take optimal values. The results show the following.

The $K_{\mathrm{m}}^{\mathrm{r}}$ curve reveals that the rib-ring stress at its inner radius apparently decreases as b/R increases. If b/R is smaller than 0.0835, the rib-ring's stress will exceed its material yielding strength. Therefore, the range $b/R = 0.0835$ to 0.10 can be considered to prevent the rib-ring material yielding and becoming too heavy. The K_{crip} curve reveals that the rib-ring crippling strength does not apparently change as b/R increases: that is, the effect of b/R on the rib-ring crippling strength is not obvious. Like the K_{crip} curve, the K_{O} curve reveals that the overall buckling strength does not apparently vary as b/R increases. Additionally, b/R does not affect the $K_{\mathrm{m}}^{\mathrm{s}}$ and K_{L} strength factors.

Accordingly, b/R is an important factor in determining the rib-ring stress. However, the effects of b/R on the other structural strengths can be ignored. Therefore, the b/R is chosen between 0.0835 and 0.10 to obtain the minimum buoyancy factor and reduce the rib-ring stress.

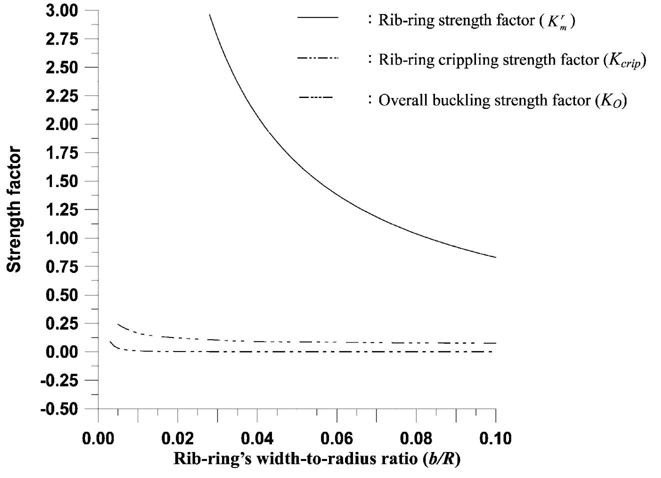

Fig. 6. The effects of the rib-ring's width-to-radius ratio (b/R) upon the structural strengths.

6.1.4. *Effects of rib-ring's inner radius-to-radius ratio* (a_i/R)

Fig. 7 shows the effects of the rib-ring's inner radius-to-radius ratio (a_i/R) upon the structural strengths of the MIS deep-submerged pressure hull, when the other three design variables take the optimal values.

The $K_{\mathrm{m}}^{\mathrm{r}}$ curve shows that the rib-ring stress at its inner radius apparently increases with a_{i}/R, and the maximum variation occurs in the range $a_{\mathrm{i}}/R = 0.50$ to 0.90.

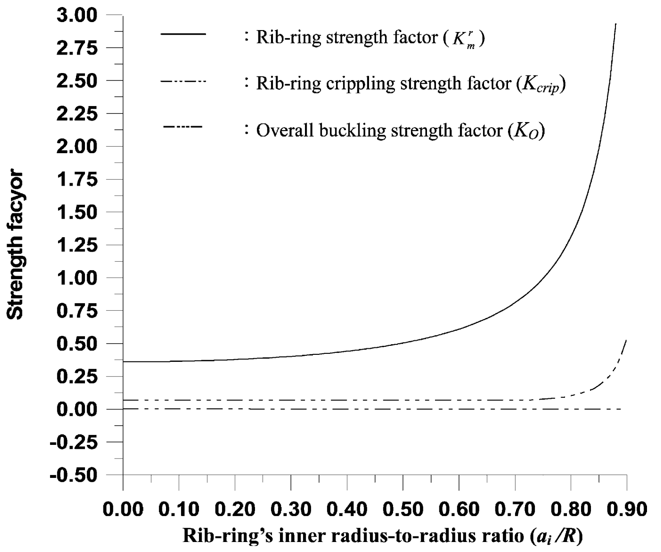

Fig. 7. The effects of the rib-ring's inner radius-to-radius ratio (a_{i}/R) upon the structural strengths.

If a_i/R exceeds 0.7518, then the rib-ring stress will exceed its material yielding strength. Moreover, when the a_i/R is smaller than 0.50, the rib-ring stress does not clearly change. Therefore, a_i/R is chosen in the range 0.50–0. 7518 to prevent the material yielding and take into account the spatial requirement. The K_{crip} curve shows that the rib-ring crippling strength does not apparently change as a_i/R increases; that is, the effect of a_i/R on the rib-ring crippling strength is not evident. The K_{O} curve reveals that the overall buckling strength of the pressure hull gradually decreases as a_i/R increases; that is, a greater rib-ring inner radius implies a poorer overall buckling strength of the pressure hull. Additionally, a_i/R does not influence the K_{m}^{s} and K_{L} strength factors.

Accordingly, a_i/R markedly affects the rib-ring stress and the overall buckling strength. However, the effects of a_i/R on the shell membrane stress, the lobar buckling strength and the rib-ring crippling strength can be disregarded. Therefore, the a_i/R can be appropriately chosen between 0.50 and 0.7518 to obtain the minimum buoyancy factor; reduce the rib-ring stress and increase the overall buckling strength.

6.1.5. Effects of angle of intersection of the shell (α)

Fig. 8 indicates the effects of the angle of intersection of the shell (α) upon the structural strengths of the MIS deep-submerged pressure hull, when the other three design variables take their optimal values.

The K_{m}^{r} curve shows that the rib-ring stress at its inner radius obviously decreases as the angle of intersection of the shell increases. If the angle of shell intersection is below 69.8°, then the rib-ring stress will exceed its material yielding strength to induce yielding. Therefore, this finding suggests that the effect of the angle of intersection of the shell on the rib-ring stress is an essential factor. The K_{L} curve shows that the lobar buckling strength in the shell does not significantly increase with the angle of intersection of the shell. If the angle is less than 69.8°, then the

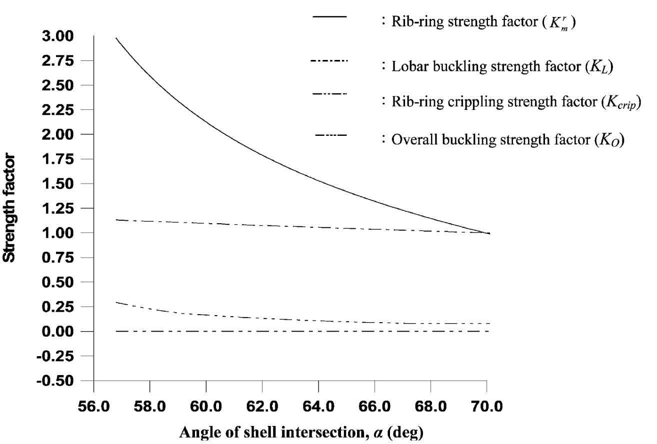

Fig. 8. The effects of the angle of intersection of the shell (α) upon the structural strengths.

lobar buckling strength cannot resist the external hydrostatic pressure load, and the local buckling of the shell occurs. This observation reveals that the angle is a principal factor in determining the lobar buckling strength of the shell. The K_{crip} curve shows that the rib-ring crippling strength does not apparently vary as the angle increases; that is, the angle does not strongly affect the rib-ring crippling strength. The K_{O} curve indicates that the overall buckling strength of the pressure hull gradually increases with the angle of intersection of the shell; that is, a greater angle implies greater overall buckling strength of the pressure hull. Also, the angle does not influence the $K_{\mathrm{m}}^{\mathrm{s}}$ strength factor.

Accordingly, the effects of the angle on the rib-ring stress, lobar buckling strength and overall buckling strength must be actively considered. However, the effects of the angle on the shell membrane stress and the rib-ring crippling strength can be neglected.

7. Conclusion

This paper presented the optimum design of multiple intersecting spheres deep-submerged pressure hull under hydrostatic pressure to minimize the buoyancy factor of the pressure hull. A sensitivity analysis was performed to study the effects of the design variables on the optimal structural strength design. Constraints were imposed on the buckling strengths and the material yielding failure strengths such that mechanical behavior must satisfy corresponding strength criteria. The thickness (t) of the shell, the width (b) of the rib-ring, the inner radius (a_{i}) of the rib-ring and the angle (α) of intersection of the shell are taken as design variables. The optimization was performed using the DFP search routine. Results were presented for the optimum design of a multiple intersecting spheres deep-submerged pressure hull. In the optimization, the strength factors $K_{\mathrm{m}}^{\mathrm{r}}$, $K_{\mathrm{m}}^{\mathrm{s}}$, K_{L}, K_{crip} and K_{O} were analyzed and evaluated with each design variable change. Table 2 summarizes the degree of influence of the design variables on the optimal design. This study yields the following observations.

1. Design variables b, a_{i}, and α profoundly influence strength factor $K_{\mathrm{m}}^{\mathrm{r}}$; the other design variable t heavily influences the strength factor K_{L}.
2. The influence of design variable t on $K_{\mathrm{m}}^{\mathrm{s}}$; the influence of design variable α on K_{L}, and the influence of design variables b and a_i on K_{O} all are of secondary importance.
3. Design variables b, a_{i}, and α slightly influence strength factor K_{crip}; design variables t and α barely influence strength factor K_{O}.
4. Design variable t does not influence $K_{\mathrm{m}}^{\mathrm{r}}$ and K_{crip}; design variables b, a_{i}, α do not influence $K_{\mathrm{m}}^{\mathrm{s}}$, and design variables b, a_{i} do not influence K_{L}.
5. The material yielding and the shell lobar buckling must be firstly considered on the optimum configuration of a multiple intersecting spheres deep-submerged pressure hull under hydrostatic pressure.

The results can serve as a valuable reference for designers of underwater vehicles. Future studies should consider the effects of the fluidstructure interaction, and the problems of impact and penetration of the multiple intersecting spheres deep-submerged pressure hull.

References

Allmendinger, E.E., 1990. Submersible Vehicle Systems Design. SNAME, New York.

Comstock, J.P., 1967. Principles of Naval Architecture. SNAME, New York.

Garland, C., 1968. Design and fabrication of deep-diving submersible pressure hulls. SNAME Transactions 76, 161–179.

Garzke, W.H., Yoerger, D.R., Harris, S., Dulin, R.O., Brown, D.K., 1993. Deep underwater exploration vehicles—past, present and future. SNAME Transactions 101, 485–536.

Gertler, M., 1950. Resistance Experiments on a Systematic Series of Streamlined Bodies of Revolution—For Application to the Design of High-speed Submarines, DTMB Report c-297.

Gorman, J.J., Louie, L.L., 1991. Submersible pressure hull design parametrics. SNAME Transactions 99, 119–146.

Hall, J.C., Leon, G.F., Kelly, J.J., 1991. Deep submergence design of intersecting composite spheres. Composites—Design, Manufacture and Applications, 2F1–2F12.

Harris, F.J., 1977. Private communication with Professor C.T.F Ross, University of Portsmouth, Portsmouth, UK.

Heggstad, K.M., 1982. Submarine pressure hulls. Maritime Defence, 239–242.

Leon, G.F., 1971. Intersecting titanium spheres for deep submersibles. ASCE Proceedings 97, 981–1006.

Liang, C.C., Chen, H.W., 2002. Structural optimization of fiber-reinforced sandwich cylindrical pressure hulls. Journal of the Society of Naval Architects and Marine Engineers (Taiwan).

Liang, C.C., Hsu, C.Y., Tsai, H.R., 1997. Minimum weight design of submersible pressure hull under hydrostatic pressure. Computers and Structures 63, 187–201.

Mckee, A.I., 1959. Recent submarine design practices and problems. SNAME Transactions 67, 623–652.

Muukki, T., 1990. Concept for a full ocean depth submersible. MTS Journal 24, 74–78.

Nash, W.A., 1995. The Structural Mechanics, Analysis and Design of Powered Submersibles. Elsevier Science, Inc., New York.

Ness, C.C., Simpson, W.M., 2000. A new submarine paradigm. Naval Engineers Journal, 143–151.

Reynolds, T., Lomacky, O., Krenzke, M., 1973. Design and analysis of small submersible pressure hulls. Computers and Structures 3, 1125–1143.

Ross, C.T.F., 1987. A novel submarine pressure hull design. Journal of Ship Research 31, 186–188.

Ross, C.T.F., 1996. Design of a ring-stiffened corrugated pressure hull. In: Engineering Systems Design and Analysis Conference, Vol. 8. ASME, pp. 37–40.

Shankman, A.D., 1968. Materials for hydrospace pressure hulls, present and future. Ocean Systems Operations of North American Rockwell Corporation, California, pp. 1–17.

Takagawa, S., 1995. Advanced technology used in Shinkai and full ocean depth ROV Kaiko. MTS Journal 29, 15–25.

Vanderplaats, G.N., 1985. A Fortran program for automated design synthesis, Version 1.10. Engineering Design Optimization, Inc., Santa Barbara, CA.

Watson, W., 1971. The design, construction, testing, and operation of a deep-diving submersible for ocean floor exploration. SNAME Transactions 79, 405–439.

Yang, M.F., Liang, C.C., Chen, C.H., 1992. A rational shape design of externally pressurized torispherical dome ends under buckling constraints. Computers and Structures 43, 839–851.

Yuan, K.Y., Liang, C.C., Ma, Y.C., 1991. Investigation of the cone angle of a novel swedged-stiffened pressure hull. Journal of Ship Research 35, 83–86.